International Journal of Geo-Information

MDPI

Article

Spatio-Temporal Change Detection of Ningbo Coastline Using Landsat Time-Series Images during 1976–2015

Xia Wang [1], Yaolin Liu [1,2,*], Feng Ling [3,4], Yanfang Liu [1,2] and Feiguo Fang [1]

1 School of Resource and Environmental Science, Wuhan University, Wuhan 430079, China; wangxia2015@whu.edu.cn (X.W.); yfliu610@163.com (Y.L.); 2012301120025@whu.edu.cn (F.F.)
2 Key Laboratory of Geographic Information System, Ministry of Education, Wuhan University, Wuhan 430079, China
3 Institute of Geodesy and Geophysics, Chinese Academy of Sciences, Wuhan 430077, China; lingf@whigg.ac.cn
4 School of Geography, University of Nottingham, University Park, Nottingham NG7 2RD, UK
* Correspondence: yaolin610@163.com; Tel.: +86-27-6877-8650

Academic Editors: Jamal Jokar Arsanjani and Wolfgang Kainz
Received: 12 December 2016; Accepted: 25 February 2017; Published: 2 March 2017

Abstract: Ningbo City in Zhejiang Province is one of the largest port cities in China and has achieved high economic development during the past decades. The port construction, land reclamation, urban development and silt deposition in the Ningbo coastal zone have resulted in extensive coastline change. In this study, the spatio-temporal change of the Ningbo coastlines during 1976–2015 was detected and analysed using Landsat time-series images from different sensors, including Multispectral Scanner (MSS), Thematic Mapper (TM), Enhanced Thematic Mapper Plus (ETM+) and Operational Land Imager (OLI). Fourteen individual scenes (covering seven phases) of cloud-free Landsat images within the required tidal range of ±63 cm were collected. The ZiYuan-3 (ZY-3) image of 2015 was used to extract the reference coastline for the accuracy assessment. The normalised difference water index (NDWI) and the modified normalized difference water index (MNDWI) were applied to discriminate surface water and land features, respectively. The on-screen digitising approach was then used to further refine the extracted time-series coastlines in the period from 1976 to 2015. Six relevant indices, length, length change, annual length change, fractal dimension (FD), average net shoreline movement (NSM) and average annual NSM, were calculated to analyse and explore the spatio-temporal change features of Ningbo coastlines. Results show that the length of the Ningbo coastlines increased from 910 km to 986 km, and the value of FD increased from 1.09 to 1.12, and the coastline morphology changed from sinuous to straight. The average NSM increased from 187 m to 298 m and the average annual NSM reached 85 m/year, indicating the advance of coastlines towards the sea at a high level. The spatio-temporal change patterns also varied in different areas. In Hangzhou Bay, significant advancement along the coastlines was experienced since 2001 mainly because of urban construction and land reclamation. In Xiangshan Bay, the forces of nature played a major role in coastline dynamics before 2008, whilst port construction, urban construction and island link projections moved the coastlines towards the sea. The coastline changes of Sanmen Bay were affected by the interaction of nature and human activities. All these observations indicate that forces of nature and human activities were the two important influential factors for the observed coastline change. In this case, the coastline complexity variation was considered responsible for various coastline patterns change of the Ningbo coast. In addition, erosion and accretion occurred in turn because of forces of nature and human activities, such as urban development and agricultural exploitation.

Keywords: coastline change; spatio-temporal pattern; Ningbo; Landsat; normalized difference water index

1. Introduction

Coastal zones around the world are vulnerable places that require special attention because of their intensified natural and anthropic disturbances. Areas adjacent to the sea are exposed to various natural phenomena, such as erosion, saltwater intrusion, subsidence, tsunamis and flood caused by surges and rivers [1,2]. The population living around the coastal (within 100 horizontal kilometres and 100 vertical metres from coastlines) was approximately 23% of the global population in 1990 [3], and the population numbers and densities were continually rising in the past decades. Human activities and large scale construction, such as harbour construction, fishery production and breeding industry, significantly affect the gulf shape and the coastline length [4,5]. Notably, coastal zone change has a significant effect on coastal ecosystem and species diversity, as well as the socio-economic consequences for local residents and tourism [6,7]. All these disturbances emphasise the need to create effective plans and scientifically manage coastal zones for sustainable coastal development. Moreover, monitoring the coastline spatio-temporal change position helps us to understand the coastal response to contemporary climate changes and human activities [8,9].

Coastline change analyses are usually conducted using ground survey and aerial photogrammetry techniques [10,11]. However, both methods are time consuming and costly, thereby resulting in difficulty of monitoring coastal dynamics at a large scale. With the development of satellite techniques, remote sensing has become a suitable tool to monitor coastal dynamics in a fast and cost effective way. Remote sensing images of high spatial resolution, such as SPOT, IKONOS and QuickBird, have been used for coastline change monitoring. For example, Chen et al. used multi-temporal SPOT images incorporating the associated tidal height dataset to detect coastline changes [12]. Di et al. demonstrated that IKONOS Geo stereo images can be used to extract coastline positions with high accuracy [13]. Puissant et al. proposed a new approach to extract coastlines by using spatial and spectral pattern in Quickbird multispectral images [14]. Apart from optical satellite images with high spatial resolution, Lee et al. [15], Niedermeier et al. [16], Liu et al. [17,18], Dellepiane et al. [19] and Baselice et al. [20] also applied synthetic aperture radar (SAR) images to detect coastline changes, because SAR images are free from weather condition. These data sources, including optical and SAR satellite images, can provide coastline detection results with fine spatial resolution at a high accuracy level. However, the cost is prohibitively high for frequent observations over large areas [8]. Moreover, the temporal resolution of remote sensing images with fine spatial resolution is low, thereby limiting the long-term monitoring opportunities of coastline changes. Satellite images obtained from Advanced Very High Resolution Radiometers (AVHRR), Moderate Resolution Imaging Spectrometer (MODIS) or Medium Resolution Imaging Spectrometer (MERIS) can monitor coastlines with a fine temporal resolution; however, their spatial resolutions are significantly coarse to extract the subtle variability of coastline changes, and the estimation results usually have high uncertainty [8].

Landsat series images from different sensors, including Multispectral Scanner (MSS), Thematic Mapper (TM), Enhanced Thematic Mapper Plus (ETM+) and latest Operational Land Imager (OLI), are potentially suitable for monitoring coastline changes in large areas. They provided observations of the study areas at a relatively fine spatial resolution of 30 m since 1972 [21]. The Landsat series images became evident since the public availability of the United States Geological Survey (USGS) in 2008. Up to date, many researchers have applied Landsat series images to extract the coastline changes of different study areas. For example, Kevin et al. applied Landsat TM imagery covering the Nile Delta coast in 1984, 1987 and 1991 to detect the position changes of the coastline [15]. Ryu et al. [22] applied Landsat TM images to investigate which band is effective for waterline extraction in tidal flat. Chen et al. [23] integrated Landsat MSS and TM images to monitor the dynamics of coastal zones,

such as coastline movement, urban expansion, land-use change, migration of shoals and deep-water channels. El-Asma et al. tracked the coastline position in the Nile Delta and estimated the remarkable changes of the Manzala lagoon surface area using Landsat MSS and TM images [24]. Li et al. used all available TM and ETM+ images from 1984 to 2013 to monitor the dynamics of a muddy coastline in western Florida [8]. Dewi et al. detected the coastline changes from multi-temporal images of Landsat TM, ETM+ and OLI by using a developed fuzzy method [10].

Landsat series images enable effective extraction of coastlines. The spectral water indices based on water body mapping methods are widely used for coastline extraction from Landsat images because of their reliability, user friendliness and low computation cost [25]. In the past decades, different water indices have been developed for water body mapping. McFeeter [26] proposed the popular normalised difference water index (NDWI) using a ratio of the green and the near-infrared (NIR) bands to enhance the presence of water features in remotely sensed imagery. Jain et al. [27] and Hui et al. [28] applied NDWI to model coastline spatio-temporal changes using multi-temporal Landsat series images. Although NDWI can enhance water information effectively in most cases, the index is sensitive to built-up features and often results in over-estimation of water bodies [29]. Therefore, Xu [29] developed a new index, namely as modified normalized difference water index (MNDWI), by improving the NDWI with the substitution of the middle-infrared (MIR) band, such as Landsat TM band 5, for the NIR bands. Considerable previous research has demonstrated that MNDWI can enhance water features and extract water bodies with higher accuracy than NDWI [24,28,30,31]. MNDWI is thus widely used for coastline extraction [11,24].

Ningbo is a vice-provincial city in China, locating in the southeast coast. Coastlines in Ningbo have changed dramatically in the past decades. As an intersection of the 21st Century Maritime Silk Route and Yangtze River Economic Zones [32,33], Ningbo is not only the core area of marine economy development in the Zhejiang Province of China, but also an important gateway for economic and cultural exchanges in Asia Pacific. The increasing connection with the world through economy and culture has accelerated the urban development of Ningbo. The development of the Ningbo coastal areas also became vital, especially after China's reform and opening up in 1978. In addition, Ningbo has been paying much attention to promoting the comprehensive port development as an international distribution and logistics centre. The abundant marine resources attracted more people's attention and developed into a set of tourism and leisure. Meanwhile, the diverse natural environment creates a complex coastal ecosystem for the Ningbo coast. The different kinds of harbours, estuaries and headlands in the coastal zone make the features of Ningbo coastline unique. Specifically, the famous Qiantang River funnel-shaped estuary separates Ningbo in the south and Shanghai in the north. The estuary suffered from erosion mainly in the north and accretion mainly in the south under the long-term effects of tides and waves or sediment transport along the shore. The coasts nearby the Yong River (the only river channel into the sea of the Ningbo coast) are mainly muddy coasts and partially rocky coasts, which are readily available. The coastlines of Ningbo experienced a series of changes during the past decades with the development of social and natural conditions of Ningbo. Thus, monitoring the Ningbo coastline dynamics over time is important.

In this study, the coastline changes of Ningbo over a large time span (1976–2015) were detected based on Landsat time-series images using the spectral water indices (NDWI and MNDWI). The past and present conditions of the coastline were analysed by estimating the change metrics of the coastline length, length change, annual length change, fractal dimension (FD), average net shoreline movement (NSM) and average annual NSM. This study could differentiate the major natural and anthropogenic factors controlling the coastline changes and facilitate the sustainable development of the coastal zone for proper utilisation.

2. Study Area

Ningbo is located close to the eastern coast of China and the southeast corner of the Yangtze River [34], as shown in Figure 1. The topography of Ningbo is higher in the southwest and lower in

the northeast, with an average elevation of approximately 4 m above the mean sea level. Ningbo has a subtropical monsoon climate. The mean annual temperature, precipitation and pan evaporation in the area are 16.4 °C, 1480 mm and 820 mm, respectively. Two main rivers, the Qiantang River (a branch of the Yangtze River) and the Yong River, drain through Ningbo eastward into the East China Sea. The tide regime in the Qiantang River is a regular semidiurnal tide with mean and max amplitudes of 4 m and 8.93 m in the estuary [33], respectively. Influenced by the topography, the world-famous tidal bore exists. The annual runoff is nearly 38,640 km^3, which mainly occurs in June. By contrast, the Yong River has a relatively narrow channel with a micro-tide.

There are two harbours and one gulf inside Ningbo, namely, Hangzhou Bay, Xiangshan Bay and Sanmen Bay (Figure 1). Hangzhou Bay is the offshore section in the Qiantang River that exhibits a typical funnel shape. The funnel shape of the bay leads to the strong deformation of tidal waves and strengthens the tidal current. The two characteristics significantly influenced the geomorphological processes and resulted in erosion in the north and sedimentation in the south of Hangzhou Bay [35]. Xiangshan and Sanmen Bays are important sea cultivation regions in Ningbo and are typical semi-enclosed bays [36]. Xiangshan Bay is a long and narrow bay, bordering Hangzhou Bay in north and adjacent to Sanmen Bay in the south and the Zhoushan Archipelago in the east [37,38]. The tidal waves that result from the prevailing wind coming from the east of East China Sea most of the year become stationary waves because of being blocked by the Liuheng Island, one of Zhoushan Archipelago in the mouth of Xiangshan Bay [37]. In addition, Xiangshan Bay becomes an ideal deep-water harbour for ships because of being surrounded by hills. Sanmen Bay is also surrounded by mountains on three sides and faces the East China Sea in the southeast.

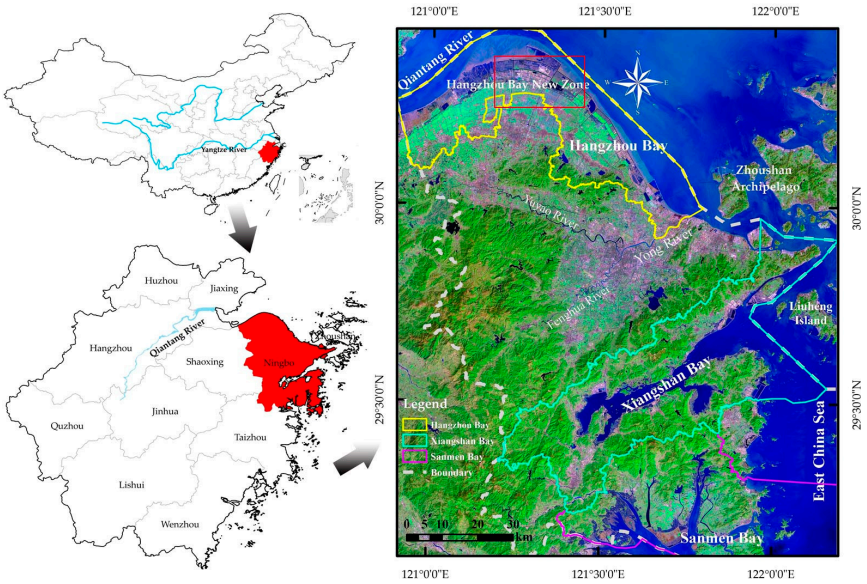

Figure 1. Geographic location of the study area and the Landsat OLI image of Ningbo as a false colour composite image (R: band 7, G: band 5, B: band 3).

A regional development plan has been formulated for the development of the three relatively independent economic regions based on the administrative division and the characteristic resources of the three bays [38–40]. Eventually, the south partial silting-up action that resulted from tide and wind created the splendid Hemudu Culture and developed the famous Sanbei Riffle with a width of 2–6 km. In the recent three decades, a set of development and construction activities has been implemented in the Sanbei Riffle. The popular Hangzhou Bay New Zone is included in this area. The population growth and urban constructions facilitated the significant land cover changes in the area since the foundation of the new zone in 2001. Abundant marine resources provide Xiangshan Bay with comprehensive functions that integrate aquaculture, ecology, tourism and marine fishery.

Marine fishery is the economic sustenance of the residents near the bay. For a long time, promoting the common development of industry, tourist and organic agriculture along the coast based on its resource advantages has driven the land use changes of Sanmen Bay coastal zone.

3. Data and Methodology

3.1. Data Sources

Landsat series images from 1976 to 2015 were used as data sources to analyse the Ningbo coastline. Large scale horizontal location variabilities at different recording times generally exist because of the tidal fluctuation, especially for a coastline with a gentle slope [7,41]. The time-series satellite datasets must be collected at similar tidal levels to compare the coastlines at different times. The near-shore bottom slope of the Ningbo coast ranges from around 21‰ to 56‰. The tidal difference between the Ningbo coastline must be no more than ±63 cm to maintain the error of Landsat images at less than one pixel (a spatial resolution of 30 m) [42].

Based on the data availability and tidal level constraint, 14 cloud-free Landsat series images within the required tidal range of ±63 cm were selected in this study. Landsat images of two similar temporal periods were used to compose one image mosaic, which covers the entire Ningbo coastal zone for each phase (Table 1). Seven phases of the 14 scenes of Landsat series images, including 4 Landsat MSS images, 6 Landsat TM images, 2 Landsat ETM+ images and 2 Landsat OLI images in 39 years (from 1976 to 2015) were used to detect the Ningbo coastline spatio-temporal changes. All the Landsat series images were downloaded in the GeoTIFF format from the United States Geological Survey (USGS) Earth Explorer Website (http://earthexplorer.usgs.gov/). These Landsat datasets constitute the useable database of good quality (level 1 product), free of clouds (at least covering the coastlines of interest) and sensor defects, such as striping or banding. Further information about the specifications of satellite data used in the study is provided in Table 1.

Table 1. Specifications of the selected Landsat time-series images.

Phase	Image Type	Acquisition Day	Path	Row	Local Time (UTC)	Tidal Level (cm)	Tidal Difference (cm)
1976	Landsat-2 MSS	7 January 1976	127	39	1:40	208	-
	Landsat-2 MSS	7 January 1976	127	40	1:40	208	-
1983	Landsat-4 MSS	9 December 1983	118	39	1:54	208	0
	Landsat-4 MSS	9 December 1983	118	40	1:54	208	0
1990	Landsat-5 TM	4 December 1990	118	39	1:45	158	−50
	Landsat-5 TM	4 December 1990	118	40	1:45	158	−50
1996	Landsat-5 TM	18 November 1996	118	39	1:48	156	−52
	Landsat-5 TM	18 November 1996	118	40	1:48	156	−52
2001	Landsat-7 ETM+	24 November 2001	118	39	2:14	209	1
	Landsat-7 ETM+	24 November 2001	118	40	2:14	209	1
2008	Landsat-5 TM	5 December 2008	118	39	2:09	148	−60
	Landsat-5TM	5 December 2008	118	40	2:09	148	−60
2015	Landsat-8 OLI	12 March 2015	118	39	2:25	154	−54
	Landsat-8 OLI	12 March 2015	118	40	2:25	154	−54

3.2. Methodology

The research methodology included: (1) image pre-processing; (2) coastline feature extraction; and (3) coastline change estimation. The flowchart of the specific processing of spatio-temporal change detection of the Ningbo coastline during 1976–2015 is shown in Figure 2.

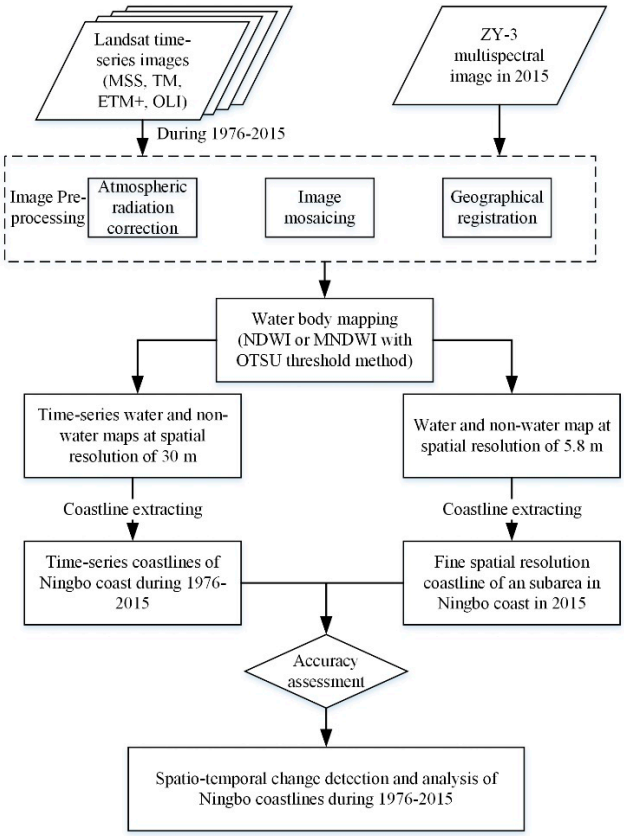

Figure 2. Flowchart of spatio-temporal change detection of Ningbo coastline during 1976–2015.

3.2.1. Image Pre-Processing

In this study, all Landsat images were radiometrically and geometrically corrected with the same projection coordination system (UTM projection, WGS-84 reference system). The at-sensor radiance (digital number, ND) values were converted to surface reflectance with the FLAASH model in the ENVI software to reduce the atmospheric effects. The spatial resolution of MSS image is 60 m, while that of TM/ETM+/OLI image is 30 m. In order to unify the spatial scale of MSS and TM/ETM+/OLI images, four MSS images from 1976 and 1983 were resampled to 30 m by the nearest neighbourhood resampling method. Two Landsat scenes with different rows needed to be mosaicked to cover the study area because of the wide range of the Ningbo coast and the limited scene coverage of Landsat MSS/TM/ETM+/OLI images. The image mosaic was carried out with ENVI 5.1 version software, thereby obtaining a composed image for the entire Ningbo coastal zone. Moreover, image-to-image registration method in ENVI was applied for the geometric correction of the Landsat time-series images [43]. The Landsat OLI image in 2015 was used as the reference for the other images, and the registration errors of all images were within one pixel (less than 30 m). Specially, the mean registration errors for MSS, TM, and ETM+ are 0.81 pixels, 0.56 pixels and 0.43 pixels, respectively.

3.2.2. Coastline Extraction

In this study, the spectral water indices based on normalised difference arithmetic operations, namely, NDWI and MNDWI, were used to delineate the water body areas because of their efficiency and convenience. A threshold adjustment method called OTSU algorithm was applied to the NDWI and MNDWI images [44]. This method provided dynamic and variational thresholds based on different regions in different phases [45]. Subsequently, the coastlines of the different phases covering the study area were extracted from the water body maps.

Producing Spectral Water Indices

NDWI was proposed by McFeeters (1996) for water resource assessment. An NIR band and a green band are used to enhance the discrepancies between surface water and non-water features [26]. NDWI [26] is defined as

$$\text{NDWI} = \frac{\rho_{GREEN} - \rho_{NIR}}{\rho_{GREEN} + \rho_{NIR}} \quad (1)$$

where ρ_{GREEN} is the reflectance value of the green band and ρ_{NIR} is the reflection value of the NIR band. The two bands are selected to: (1) maximise the reflectance of water using the green wavelength; (2) minimise the low reflectance of water feature in NIR; and (3) take advantage of the high reflectance of vegetation and soil features in the NIR band [44,45]. As a result, sensors that have a green band and an NIR band can be used to calculate this index. Accordingly, positive values of water features and zero or negative values of terrestrial vegetation and soil can be obtained. Thus, the presence of water is enhanced significantly, whilst the presence of terrestrial vegetation and soil is suppressed or eliminated [26].

However, confusions between water and non-water features always exist in the application of NDWI to water areas with built-up backgrounds. As previously reported in [29,30,44,46], the reflectance pattern of build-up features in the green band and the NIR band are similar with that of water, and the accuracy of extracting water is reduced by mixed build-up features. NDWI is thus modified by substituting the MIR band for the NIR band to remove the build-up feature noise when applying the NDWI index to water extraction. The derived new index is called MNDWI [29], which is expressed as

$$\text{MNDWI} = \frac{\rho_{GREEN} - \rho_{MIR}}{\rho_{GREEN} + \rho_{MIR}} \quad (2)$$

where ρ_{MIR} is the reflectance of the MIR band. The calculation of MNDWI can result in negative values of build-up lands, and the positive ratio value of water can be higher than that from NDWI. Such results are attributed to the specific characteristic that water absorbs more MIR light than NIR light.

As we all know, MSS is a four-band sensor, consisting of one green band, one red band and two NIR bands. Thus, only NDWI can be computed using MSS images for the missing of MIR band. TM image has the following wavebands: bands 1–3 covering the visible spectrum in the blue, green and red; band 4 with a wavelength range in the NIR; bands 5 and 7 covering the MIR; and band 6 covering the thermal infrared (TIR). The ETM+ sensor detects reflected radiation from the Earth's surface in the same seven bands as the TM and has an additional panchromatic (band 8). The OLI instrument provides enhancement from the prior ETM+ sensor and has two additional spectral bands, namely, coastal aerosol band (band 1) and cirrus band (band 9). Therefore, both the indices of NDWI and MNDWI can be calculated on TM, ETM+ and OLI images. Ultimately, NDWI was applied to the MSS images, and MNDWI was applied to the TM/ETM+/OLI images (Table 2). The NDWI or MNDWI images of the different Landsat images at different years are shown in the second column of Figure 3. The subarea image of Hangzhou Bay was used in this example.

Table 2. Water indices, normalised difference water index (NDWI) and modified normalized difference water index (MNDWI), for different Landsat image types.

Phase	1976	1983	1990	1996	2001	2008	2015
Image Type	MSS	MSS	TM	TM	ETM+	TM	OLI
Index	NDWI	NDWI	MNDWI	MNDWI	MNDWI	MNDWI	MNDWI

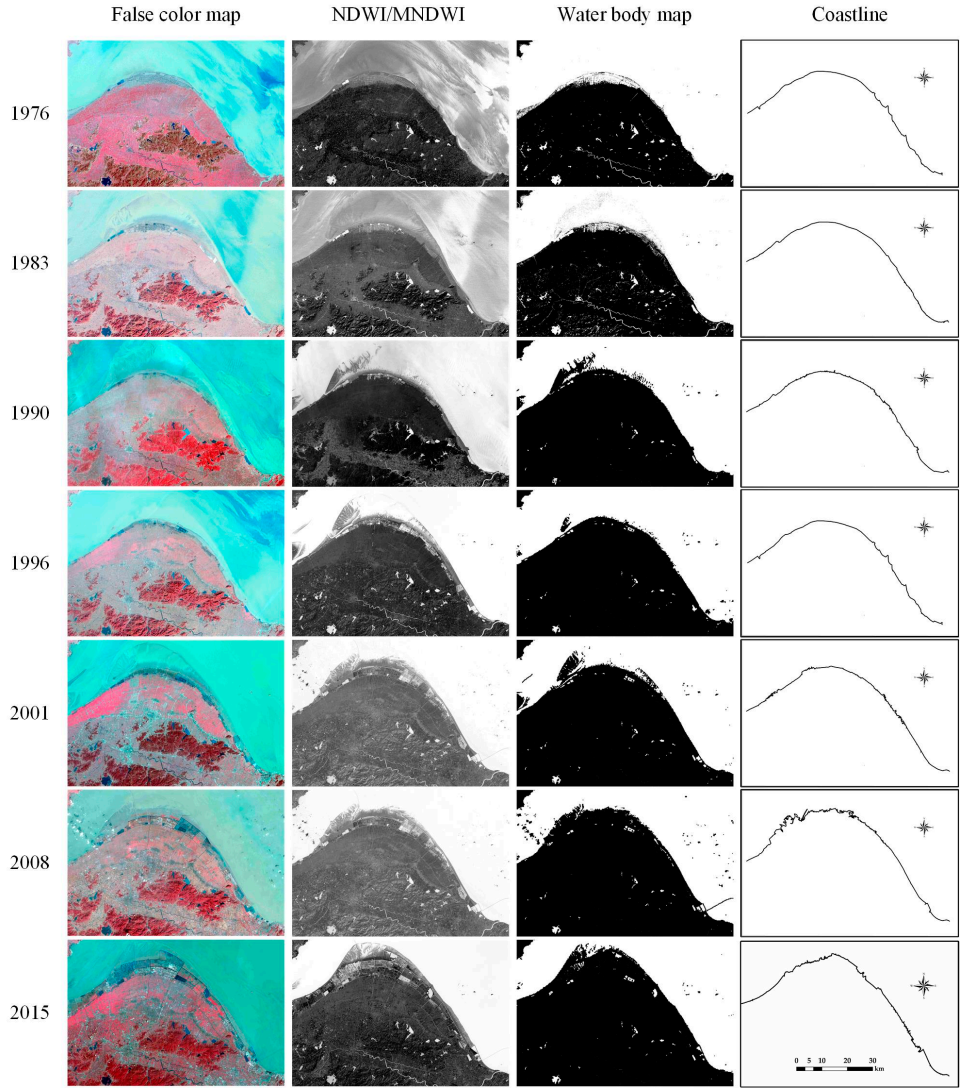

Figure 3. Process of coastline extraction in Hangzhou Bay (the first column is the false colour composite image (R: band 7, G: band 5, B: band 3).

Water Body Mapping Using the OTSU Algorithm

Using the produced NDWI and MNDWI images, two classes (land and water) were then extracted by a threshold segmentation method in this section. However, achieving a certain optimal threshold for extracting water bodies from NDWI and MNDWI images was a challenge. The threshold values of McFeeter's NDWI and Xu's MNDWI are always set to zero, but the threshold is not a constant value and changes depending on the subpixel land-cover components [47]. A threshold adjustment method was therefore required to achieve an accurate extraction of the coastline. Otsu's method, proposed by Nobuyuki Otsu [48], is a dynamic method that has been successfully used to partition the input raster image into homogeneous land and water regions through minimising the intra-class variance [21,44,45]. Assuming t represents the threshold value, ranging from a to b ($-1 \leq a \leq b \leq 1$), the optimal threshold value t^* can be obtained by the following algorithm:

$$\begin{cases} \sigma^2 = P_{nw} \cdot (M_{nw} - M)^2 + P_w \cdot (M_w - M)^2 \\ M = P_{nw} \cdot M_{nw} + P_w \cdot M_w \\ P_{nw} + P_w = 1 \\ t^* = Arg \underset{a \leq t \leq b}{Max} \left\{ P_{nw} \cdot (M_{nw} - M)^2 + P_w \cdot (M_w - M)^2 \right\} \end{cases} \quad (3)$$

where σ is the between-class variance of non-water and water pixels, and P_{nw} and P_w are the possibilities of pixel subjects to the non-water and water classes. M_{nw} and M_w represent the mean values of non-water and water pixels, whilst M is the mean value of the entire image.

Using the OTSU algorithm, the ideal values of threshold t^* can be achieved to distinguish water and non-water pixels. The pixels with values equal or higher than the threshold value referred to water. Otherwise, the pixels were classified as non-water objects. The water body maps (the third column of Figure 3) were produced for different NDWI and MNDWI images using their own optimal threshold values.

Coastline Extracting from Water Body Maps

Raster-to-vector conversion processes were performed using the ArcGIS Software to track the coastlines from the water body binary maps generated by the steps mentioned above. Furthermore, a careful on-screen visual inspection correction was applied to ensure the accuracy and reliability of the coastline extraction results [24]. The last column of Figure 3 illustrates the shape of the coastlines (Hangzhou Bay) from 1976 to 2015.

3.2.3. Coastline Change Estimating

A quantitative analysis of the pattern and metrics of spatio-temporal coastline changes must be performed on the individual time-series coastlines extracted from the Landsat images. Six indices including length, length change, annual length change, FD, average NSM and average annual NSM, were utilised as the quantitative spatio-temporal change indicators. The ArcGIS software can estimate the indices of length, length change and annual length change. More information about the indices of FD, average NSM and average annual NSM are presented as follows.

Fractal Dimension

FD is widely used to characterise roughness and self-similarity in the measurement, analysis and classification of shape and texture [49]. FD can be calculated using the divider and box-counting methods [50]. The latter is popularly used because of its efficiency and user friendliness. The box-counting method involves covering the curve with a square grid and with variable lengths. The size of the square grid is denoted as ε and the number of grids covering the curves is denoted as N. According to fractal theory, the estimation of FD can be converted to the following equivalent equation:

$$\log N = -D \log \varepsilon + A \tag{4}$$

where A is a constant and D is the FD of the curve. If a change in the value of ε exists, then a corresponding value of N is generated accordingly. Without considering the value of A, the value of D can be obtained by the least square method.

Transect-from-Baseline Approach

The principle of the transect-from-baseline approach is based on the assumption that the distance associated with this translation is a measurement of shoreline change if the position of a point on one shoreline shifts to a corresponding position on the other time-series shoreline [51]. The Digital Shoreline Analysis System (DSAS) [52], a free extension for ArcGIS, was utilised to measure the distance of shoreline migration through constructing transects automatically from a baseline to a set of historical shoreline data [53]. A baseline is necessary for this operation, and this baseline must be established adjacent to the general trend of the shoreline series [51]. An efficient way to create the baseline is to generate a parallel matching of the general trend of the set of shorelines. As reported in [51], the baseline based on a buffer distance of 1000 m is the most appropriate for all coastlines. Thus, the baseline in this study was built approximately 1000 m onshore using the buffering technique and editing tool of ArcGIS. Therefore, all coastlines were located on one side of the baseline.

Using the baseline and all time-series coastlines, the DSAS analysis was performed to establish transect locations and calculate the related change statistics. The horizontal interval in the DSAS analysis was set to 500 m, and then 1060 transects were created. NSM shows the shortest distance between the oldest and newest shorelines for each transect [52]. A positive value indicates that a seaward tendency of migration occurs; otherwise, the migration moves landward.

Subdivision of the Study Area

The entire Ningbo coastlines were divided into three broad coastal sectors (Figure 1) based on the natural environment and the regional development strategy. In doing so, the time-series changes of the coastlines could be clearly analysed and presented. The three broad coastal sectors included Hangzhou, Xiangshan and Sanmen Bays. These bays present different patterns of coastline changes because of limited marine resources, environment and regional development orientation. Hangzhou Bay starts from the Qiantang River to the Yong River. Xiangshan Bay is a narrow and long semi-closed bay and is located in the middle of the Ningbo coastline. Sanmen Bay is located at the south of the Ningbo coastline.

4. Results and Discussion

4.1. Accuracy Assessment

The point-by-point comparison method [54] was used to assess the accuracy of coastline extraction results. The ZiYuan-3 (ZY-3) multispectral image with a spatial resolution of 5.8 m [55] was selected as the reference remote sensing data to extract fine subarea spatial resolution of the Ningbo coastline. The fine spatial resolution ZY-3 image was acquired at 2:43 a.m. (UTC) on 12 March 2015; this image shared nearly the same acquisition time as that of the Landsat 8 OLI multispectral images of 2015 (Table 1). In this case, the acquisition times of ZY-3 and Landsat OLI images ensure nearly similar tide levels. Before further study, ZY-3 was geometrically corrected to the OLI image with the error of 0.5 pixel of ZY-3 image. The first-order polynomial transformation and the nearest neighbour resampling models were applied in the conversion and the registration processes, respectively. Figure 4 shows that the selected subarea ZY-3 multispectral image is located within Xiangshan Bay that includes all types of coastlines. The ZY-3 multispectral image has four bands, including one NIR band and three visible bands. The NDWI index method was applied to distinguish the water bodies from other land covers. The coastline extracted from the ZY-3 image (yellow lines in Figure 4) was used as the reference coastline. A series of points (total 556) along the baseline in an interval scale of 100 m were selected as test points to validate the coastline extracted from the Landsat OLI image in comparison with the reference coastline. In order to suppress the special condition: an extended spit [56], the minimum distance between the coastline extracted from the Landsat OLI image and the reference coastline was measured [52], and it is used as an index to indicate the minimum error between extracted coastline and reference coastline. The reference coastline presented the exact position, whilst the extracted coastline presented the indicated value. The error was the difference between the true and indicated values, that is, the distance. By applying the Kolmogorov–Smirnov test [42,57], the errors were obtained within a confidence level of 95%. Specifically, the mean error between the produced coastline of the Landsat OLI images and the reference coastline of ZY-3 was 1.68 m with a standard deviation of 25.46 m. This error value is less than the size of one pixel within the Landsat images and is acceptable for the application [42].

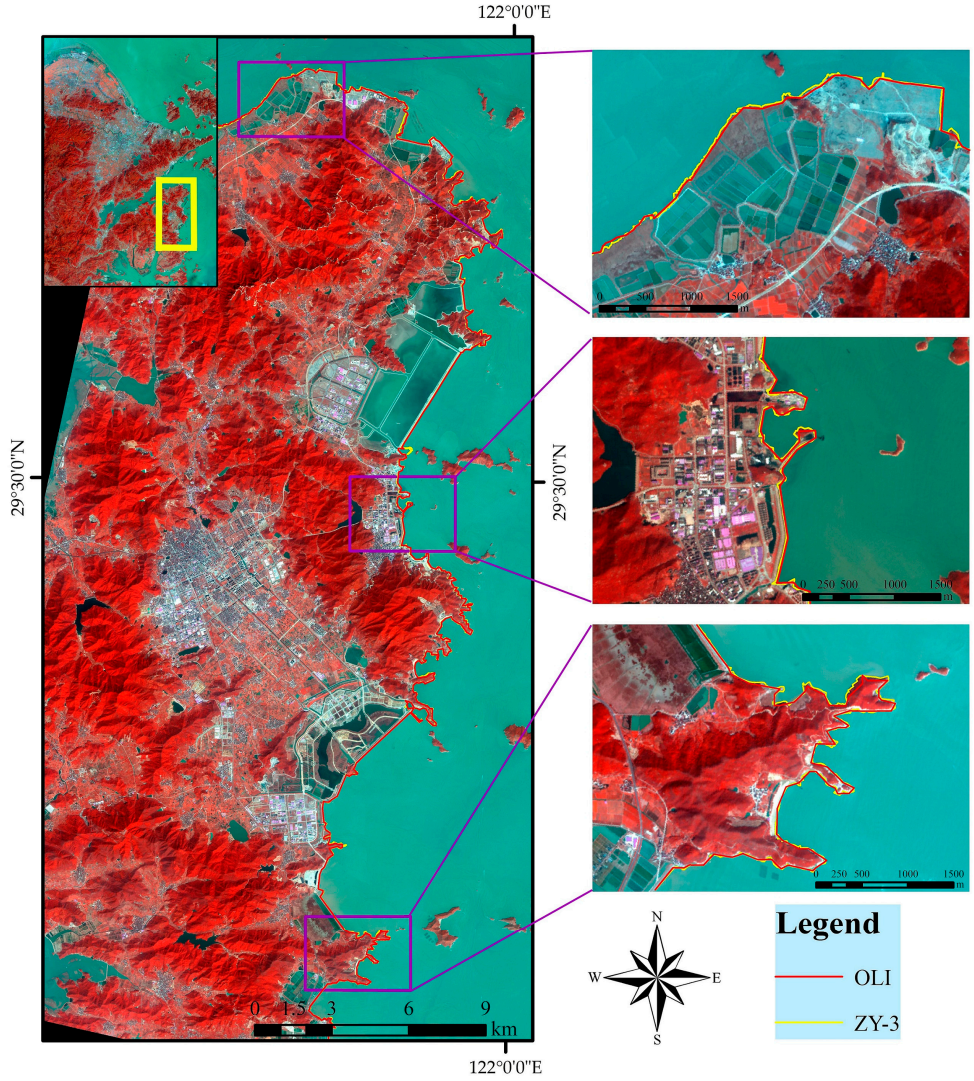

Figure 4. Coastline extracting errors between the reference coastline produced from the ZY-3 multispectral image (**yellow**) and the coastline produced from the Landsat OLI image (**red**) in 2015.

4.2. General Coastline Change

The coastlines produced by the Landsat time-series images during 1976–2015 are shown as different colour lines in Figure 5. In general, the change in the coastlines presented a trend of seaward migration. This trend was especially evident in the north and south of the study area; that is, Hangzhou and Sanmen Bays. However, long strips of coastline existed between Hangzhou and Sanmen Bays with no significant change. This result is mainly due to the highly developed ports and hardly developed bedrock coasts. The changes within Hangzhou, Xiangshan and Sanmen Bays are further discussed in the following sections.

Figure 6 shows the values of coastline length and FD during 1976–2015. Both curves showed "V" shapes with a minimum value in 1990. From 1976 to 2015, the length of the coastline changed from 807 km to 1005 km. Meanwhile, the minimum and maximum FD values were 1.07 in 1990 and 1.13 in 2008. Considering the coastline morphological feature, the coastline in 1990 became straighter than the coastlines in 1976 and 1983 because of the conversion of water bodies to agricultural lands of regular shapes. The coastline in 2008 experienced an obvious advanced process and maintained a high sinuosity. For example, the coastline within Hangzhou Bay New Zone has been advancing seaward because of urban construction, including industrial and recreational activities and housing

construction, since December 2001. The change process of FD with the increase in the coastline length was gentler than that of the coastline length. The change rate of FD was negative in some instances. The FD value in 2001 was higher than that in 2015. Notably, the coastline in 2015 was longer than that in 2001 and the difference of the coastline lengths was only 3 km. The change rate of coastline length (0.30%) was much lower than that of FD (0.73%). The coastline advancement caused by the forces of nature, such as sediment deposition, may enhance the complexity of coastline change in the region. By contrast, coastline regression may weaken the complexity, especially for muddy coasts. Human activities, such as seawall construction and agricultural land reclamation, can significantly change the coastline lengths. If this phenomenon continues in the future, then the FD value of the coastline can be approximately one. In other words, the coastline can be a straight line without inherent natural characteristics.

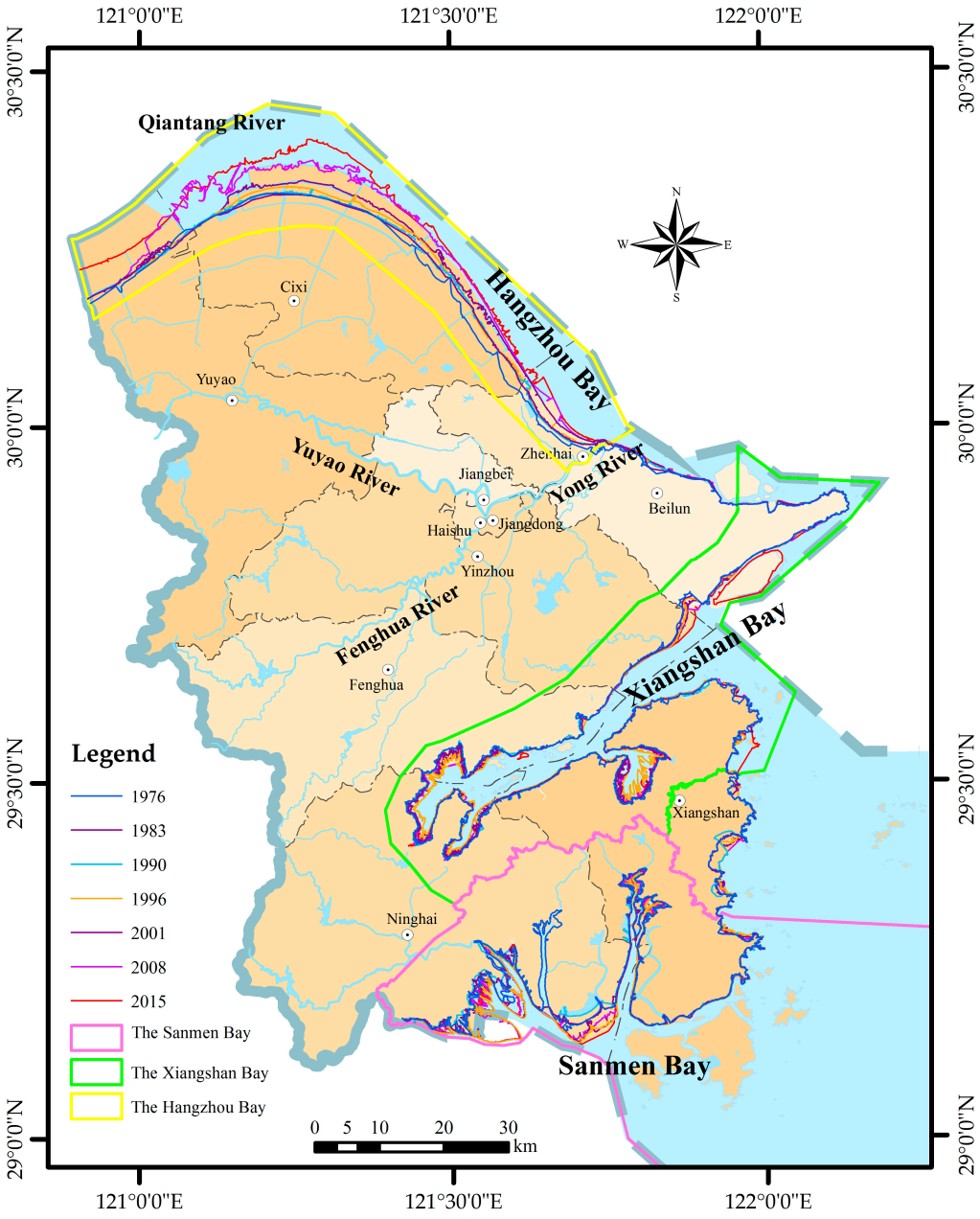

Figure 5. Coastlines of Ningbo since 1976 to 2015.

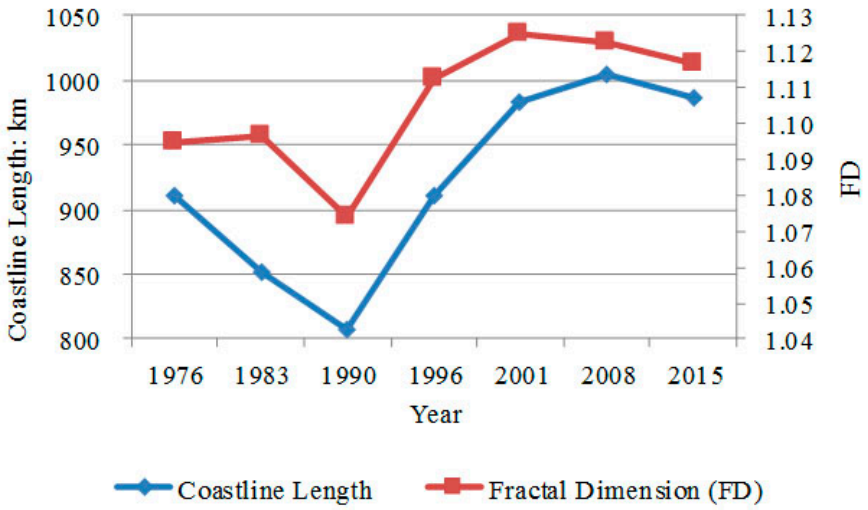

Figure 6. Changes of coastline length and FD values during 1976–2015.

Table 3 shows the coastline change information in consecutive years during 1976–2015. The three largest change rates in average were 16 km/year during 1990–1996, 15 km/year during 1996–2001 and −8 km/year during 1976–1983. The minimum decreased and increased values of the coastlines were −3 and 3 km/year, respectively. The average NSM and average annual NSM rates were positive except those from 1983 to 1990 and 1996 to 2001. The maximum average NSM was 561 m in the time frame of 1990–1996. Accordingly, the maximum average annual NSM was 85 m/year, whilst the minimum was 8 m/year during 1983–1990. From 1990 to 1996, the coastline experienced significant advancement because of the sediment deposition caused by the forces of nature in Xiangshan and Sanmen Bays. The coastlines during 2001–2008 and 2008–2015 presented significant advancement. The inverse trend was found for the coastline lengths, and the values in the above-mentioned periods were less than those during 1990–1996. The Landsat images of 2001, 2008 and 2015 show that intensive levee constructions along the coasts extended the land to water and straightened the coastlines.

Table 3. Coastline change details of Ningbo coast from 1976 to 2015.

Year	Length Change (km)	Length Change Rate (km/Year)	Average NSM (m)	Average Annual NSM (m/Year)
1976–1983	−59	−8	187	27
1983–1990	−43	−7	−53	−8
1990–1996	103	16	561	85
1996–2001	72	15	−28	−6
2001–2008	21	3	293	42
2008–2015	−19	−3	298	48

4.3. Change in a Typical Coastal Area: Hangzhou Bay

The change of the coastline position between 1976 and 2015 along Hangzhou Bay is shown in Figure 7. A total of 200 measurement points were selected along the baseline. The shortest distances of the coastline from the former year to the subsequent year were summed to produce the coastline change distance, as shown in Figure 7c. In this figure, a negative value indicates erosion and a positive value indicates accretion. The statistical analysis based on Figure 7a–c shows a remarkable increase in land areas along the coastline, especially in the northern part of Hangzhou Bay. The average annual NSM in Hangzhou Bay area was 112 m/year. Meanwhile, the length of the coastline increased by 41 km, and the change trend of the length was similar to the pattern of the FD value (Figure 7b).

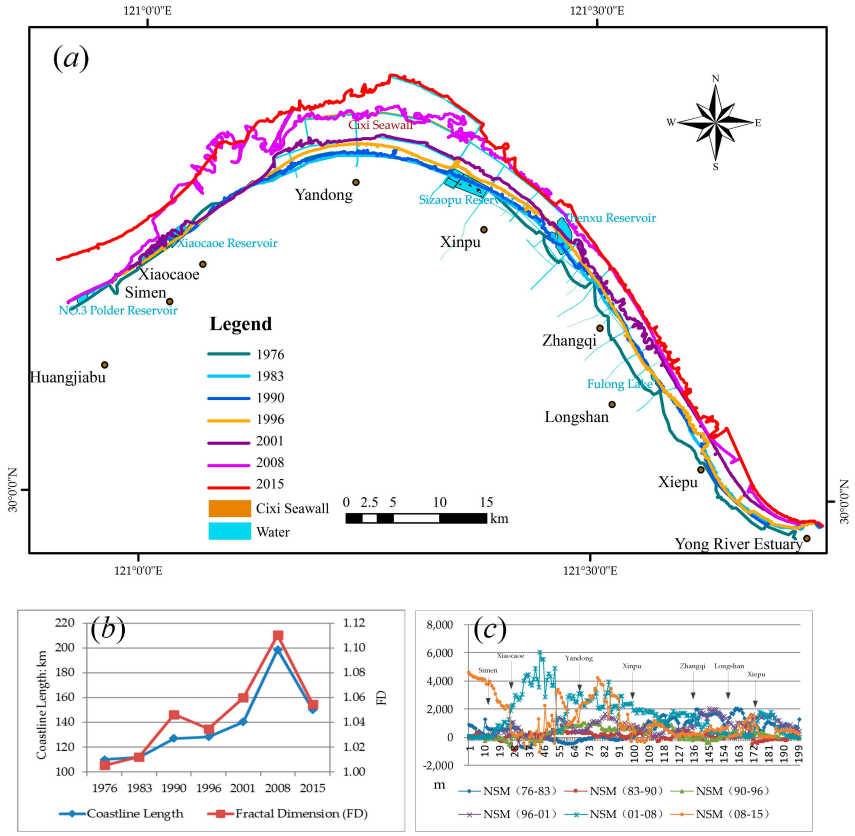

Figure 7. Illustrations of time-series coastlines of Hangzhou Bay from 1976 to 2015: (**a**) multi-temporal positions of coastlines; (**b**) changes of coastline length and fractal dimension; and (**c**) displacements along the coastlines.

During 1976–1990, the coastline was extended from 110 km to 127 km with an increased seaward displacement, and the mean coastline advance was 46 m/year. This accretion occurred mainly in the segment from Xinpu to the mouth of Yong River because of the heavy silting carried in the tide transfer of the Yangtze River and the Qiantang River and the reclamation works from Xinpu to Zhangqi and Xiepu to the mouth of the Yong River. Wherein, the average annual NSM of the coastline during 1976 and 1983 was 79 m/year and the average annual NSM of coastline during 1983 and 1990 was 10 m/year, which illustrated the step-down progress of accretion caused by the effect of human activities and relative balance of sediment deposition and erosion. From 1990 to 1996, the accretion continued and the northern part of Hangzhou Bay coastline began to present remarkable accretion, whilst the rest of the coastline exhibited stability. The average shoreline advancement was 44 m/year because several aquaculture developments existed in the coastal zone. Moreover, the construction of the Sizaopu Reservoir significantly contributed to the advancement. In addition, the main channel shifting of the Qiantang River led to a large number of sediment accumulation from Xinpu to Zhangqi [58]. The accretion continued during 1996–2001 with an average annual NSM of 148 m/year. In this processing, the forces of nature were no longer the major cause of the spatial displacement of the coastline. Human activities, including agriculture reclamation and seawall construction based on the unconsolidated soil, contributed significantly to the migration of the coastline. During 2001–2008 and 2008–2015, the coastline in Hangzhou bay exhibited significant accretions. Wherein, the average annual NSM of the coastline and the length during 2001–2008 were 226 m/year and 8 km/year. The average annual NSM of the coastline during 2008–2015 extended to 182 m/year. Meanwhile, the coastline length during 2008–2015 experienced decrease of −7 km/year. Obvious advancement was observed between the Xiaocaoe and Zhangqi coastlines during 2001–2008, and the Yandong coastline continued moving

seaward during 2008–2015. Such severe accretion was caused by the significant human activities, such as factory construction, housing construction, urban public green space construction within the seawall revetment and agriculture reclamation towards the sea, which were closely associated with the establishment of Hangzhou Bay New Area in 2001. In addition, the construction of the Cixi Seawall affected the tidal flow and the sediment discharge, for example, at the coast between the Xiaocaoe and Yandong coastlines.

4.4. Change in a Typical Coastal Area: Xiangshan Bay

The changes in the position of Xiangshan Bay coastline between the Chuanshan and Xiangshan peninsulas are shown in Figure 8. The corresponding accretion–erosion change pattern of Xiangshan Bay were different from that of Hangzhou Bay. Four dominant location displacements, including sites A, B, C and D, are illustrated in Figure 8a. The tendencies of the coastline length and FD values are presented in Figure 8b. The shortest migration distances obtained from the 484 measurement points along Xiangshan Bay coastline are shown in Figure 8c. From 1976 to 2015, the length of the coastline extended from 356 km to 424 km and the value of FD decreased by 0.04 and sharply increased after 1990. Meanwhile, the mean change distance of the coastlines was 12 m/year, which was much less than that of Hangzhou Bay. This phenomenon is due to the dynamic accretion–erosion process caused by the periodic tides and the long rocky coast.

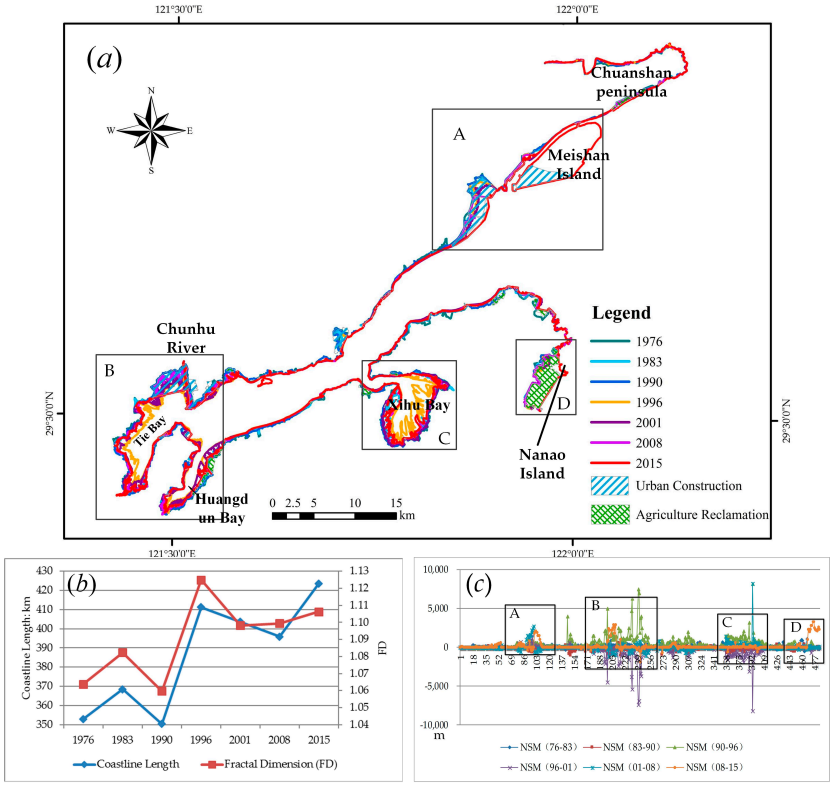

Figure 8. Illustrations of time-series coastlines of Xiangshan Bay from 1976 to 2015: (**a**) multi-temporal positions of coastlines and land exploitation projection; (**b**) changes of coastline length and fractal dimension; and (**c**) displacements along the coastlines.

From 1976 to 1990, the average shoreline migration was 2 m/year. Specifically, the average annual NSM values from 1976 to 1983 and 1983 to 1990 were 20 m/year and −17 m/year respectively. Therefore, a dynamic balance transition from accretion to erosion occurred. Between 1990 and 1996, sites B and C experienced a rapid length increase, which extended the coastline from 350 km to 411 km. Meanwhile, the value of FD increased by 0.07. During this period, alongshore sedimentation was

the dominant geophysical process for the mean shoreline progression of 83 m/year. The accretion resulted from the excessive deposition of sediment trapped on sites B and C. The mean change distance of the coastlines from 1996 to 2001 was −60 m/year, whilst the length decreased from 411 km to 403 km. Most of the erosions occurred in the three small bays of sites B and C. The comparison of the average annual NSM during 1990–1996 with that during 1996–2001 shows that the amount of accretion exceeded that of erosion. Consequently, the annual coastline progress was 12 m/year and the length of the coastline increased by 53 km during 1996–2001. From 2001 to 2008, sites A and B experienced erosion, whilst site C experienced an accretion, and the rest of the coastline exhibited a relative resistant condition because of the stable rocky coast. From 2008 to 2015, dramatic increases occurred in sites A, B and D, which were due to the island link projects in sites A and D and the artificial levee for urban construction in sites A and B. Two islands (Meishan Island in section A and Nanao Island in section D) close to the mainland were connected to the continent through the conduction of embankments and roads. In this case, the coastline position exhibited obvious migration, whilst the coastline FD value decreased for more straight coastlines. The seawall in site B completely prevented the seawater from coming in and the inland water surrounded by the seawall was converted to land. Therefore, the sinuous coastline was replaced by a straight line coinciding with the seawall.

4.5. Change in a Typical Coastal Area: Sanmen Bay

The shifts of the shoreline position along Sanmen Bay are shown in Figure 9a, and the change of the coastline length and the FD values are shown in Figure 9b. A total of 264 measurement points were selected along Sanmen Bay coastline, and the coastline change distances are shown in Figure 9c. Sites A, B and C in Figure 9a illustrate the remarkable migration along the coastline of Sanmen Bay. The average annual NSM of all the coastlines were 10 m/year. Considering the length and the FD value, the general change pattern of the coastlines was divided into three stages: the rapid decrease stage (1976–1990), the quick increase stage (1990–2001), and the small decrease stage (2001–2015).

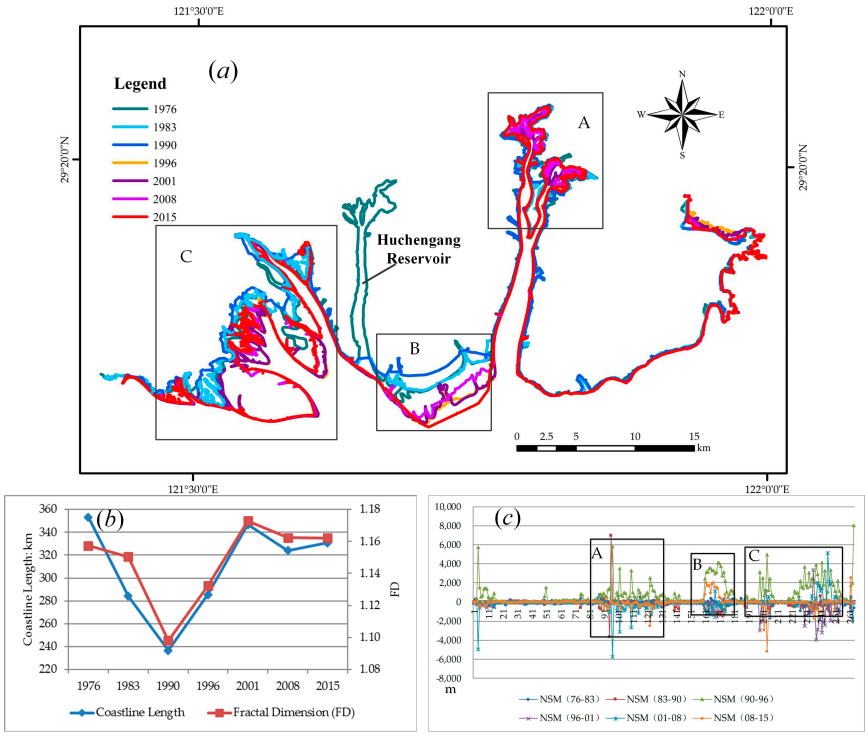

Figure 9. Illustrations of Sanmen Bay coastline from 1976 to 2015: (**a**) multi-temporal positions of coastlines; (**b**) changes of coastline length and fractal dimension; and (**c**) displacements along the coastlines.

During the period between 1976 and 1983, the coastline length decreased from 353 km to 284 km and the FD value decreased from 1.16 to 1.15. Even with the construction of the Huchengang Reservoir, the shoreline in this Bay did not change remarkably and this stage was considered the stable period. During 1983–1990, the coastline witnessed a mean erosion of –20 m/year, which mainly occurred in sites A, B and C. This phenomenon was due to the transition from accretion to erosion under the occurrence of southeast dominant wind across Sanmen Bay. From 1990 to 1996, accretion occurred with an average rate of 136 m/year in sites A, B and C. The coastline length increased from 236 km to 285 km and the FD value increased from 1.10 to 1.13. Between 1996 and 2001, erosion occurred mainly in sites B and C with an average shoreline withdrawal of −33 m/year. The local wind wave and sand loss by tidal current were the main causes of erosion in Sanmen Bay coastline. From 2001 to 2008 and 2008 to 2015, the erosion continued with an average landward migration of −13 m/year and −8 m/year, respectively. Sanmen Bay coastline length during 2001–2008 decreased by 23 km, whilst the corresponding FD variation decreased from 1.17 to 1.16. Afterwards, the coastline length and the FD value from 2008 to 2015 slightly increased. During the two periods, the coastline experienced large changes in sites B and C. From 2001, the newly built aquaculture ponds and constructions of embankment moved the coastline towards the sea and straightened the coastline. Over the entire study period, the major factors that caused the shoreline change in Sanmen Bay during 1976–2001 were the sediment deposition and erosion. The increase of agriculture lands and settlements also contributed significantly to the shoreline change in the period from 2001 to 2015.

5. Discussion

Ningbo, an important port city in China, has developed rapidly since 1970s. As a result of the forces of nature and human, the morphology of coastline is changing rapidly. For lack of previous research of coastline in Ningbo, remote sensing data help us understanding the coastline spatial displacement response to contemporary climate changes and human activities. The present research monitored the spatio-temporal coastline changes extracted from Landsat MSS, TM, ETM+ and OLI images of the Ningbo coastal zone during the period of 1976–2015. The results illustrate that significant changes occurred on the Ningbo coastline during the study period, especially on Hangzhou Bay. Specifically, the average annual NSM of Hangzhou Bay coastline was 112 m/year, which was far higher than those of the two other selected coastal areas. Besides, the length of the coastline in Hangzhou Bay increased from 110 km to 151 km in the period from 1976 to 2015. Accordingly, the FD value increased from 1.01 to 1.06. Human activities were the major factor of coastline advancement in Hangzhou Bay. Meanwhile, the main coastline displacements of Xiangshan Bay occurred in sites A, B, C and D (Figure 8). The rest of Xiangshan Bay coastlines changed slightly because of the deep-water channel and the long rocky coast. In this case, the annual spatial displacement of Xiangshan Bay coastline was only 12 m/year and the coastline length increased by 71 km in the study period. By contrast, the coastline length of Sanmen Bay decreased by 22 km with an advancement of 10 m/year during 1976–2015. The FD value of the coastline in Sanmen Bay remained at a high level with a maximum of 1.17 from 1976 to 2015, indicating that Sanmen Bay coastline pattern was more complex than those of the other investigated coastlines. Considering the coastline spatial displacement of Sanmen Bay, subsites A, B and C experienced obvious changes and were affected by natural and human factors. In summary, the erosion and accretion in the Ningbo coastline during 1976–2015 were due to natural and anthropogenic factors. Firstly, the hydrologic and geologic feature of Ningbo coast led to the rapid changes of morphology and length of Ningbo coastline by the erosion and sediment accretion. In the case, the Ningbo coastline maintained high complexity and the change tendency of the FD value was consistent with the change of length. Secondly, aquaculture development in the coastal zone and land reclamation on the muddy coast disturbed the shoreline stability by the down-drift erosion and up-drift accretion along the coast. In addition, construction of harbours and seawalls resulted in a dramatic seaward expansion. The length of the coastline was decreased because of sinuous coastline substituted by straight coastline. The same trend was observed for the FD value.

It is noteworthy that the older Landsat dataset (MSS 1976 and 1983) has a spatial resolution of 60 m, twice coarser than those of Landsat TM/ETM+/OLI images. This limitation has resulted in a relatively higher registration error, and then controlling the registration error between Landsat MSS and OLI images is critically important for the spatio-temporal extraction of Ningbo coastline. Besides, for the missing of MIR band, MNDWI cannot be used for MSS image to discriminate the land-water interface, which also increases the spatial placement discrepancy between coastlines extracted from MSS image and TM/ETM+/OLI images.

Although the spatial resolution of Landsat series dataset is suitable to monitor the spatio-temporal changes of Ningbo coastline, it is still limited to discriminate the surface water and non-water features at a higher accuracy level. Because of the limited spatial resolution of Landsat images, edge pixels likely consist of a mixture of water and non-water components. In future research, the coastline extracted at the sub-pixel level from Landsat images is of great interest to be studied. On the other hand, for the place where significant changes occurred around the Ningbo coastline during the study time, such as Hangzhou Bay, higher spatial resolution remotely sensed images should be applied to further analysis the coastline changes at finer spatial resolution. Moreover, for the places where significant changes occurred around the Ningbo coastline, it is significant to analyse land cover and land use change, and discuss the interaction between the coastline change and land cover/use change.

6. Conclusions

In this study, the spatial position of Ningbo coastline and its changing patterns during the past forty years (1976–2015) have been mapped by integrating remote sensing and GIS techniques. The results show that significant coastline changes took place in the study period. Before 2001, the force of nature played a major role for the Ningbo coastline spatial displacement, showing no drastically changes. During 2001–2015, the coastline experienced a significant advance process, especially in Hangzhou Bay. In this period, human activities produced a great impact on coastline spatio-temporal change. The results are important for understanding the spatio-temporal changes of Ningbo coastline, and would be useful for the decision-making on the Ningbo coastline land use planning.

Acknowledgments: This work was supported in part by the Special Found of Ministry of Land and Resources of China in the Public Interest under Grant No. 201511001.

Author Contributions: Xia Wang and Yaolin Liu conceived the main idea of the paper and designed and performed the experiment. Feng Ling and Yanfang Liu contributed in the modelling of water body extraction. Feiguo Fang contributed in conducting the box-counting method of fractal dimension. Xia Wang wrote the manuscript. All authors contributed in improving the paper.

Conflicts of Interest: The authors declare no conflict of interest.

References

1. Nicholls, R.J.; Small, C. Improved estimates of coastal population and exposure to hazards released. *Eos Trans. Am. Geophys. Union* **2002**, *83*, 301–305. [CrossRef]
2. Marfai, M.A.; Almohammad, H.; Dey, S.; Susanto, B.; King, L. Coastal dynamic and shoreline mapping: Multi-sources spatial data analysis in Semarang Indonesia. *Environ. Monit. Assess.* **2008**, *142*, 297–308. [CrossRef] [PubMed]
3. Small, C.; Nicholls, R.J. A global analysis of human settlement in coastal zones. *J. Coast. Res.* **2003**, *19*, 584–599.
4. Lin, L.; Pan, Z.; Kang, X.; Ye, N. The coastline extraction for Fujian province based on long time series of remote sensing image. In Proceedings of the 2013 The International Conference on Remote Sensing, Environment and Transportation Engineering, Nanjing, China, 26–28 July 2013; Atlantis Press: Amsterdam, The Netherlands, 2013; pp. 63–66.
5. Jin, D.; Hoagland, P.; Au, D.K.; Qiu, J. Shoreline change, seawalls, and coastal property values. *Ocean Coast. Manag.* **2015**, *114*, 185–193. [CrossRef]

6. Arkema, K.K.; Guannel, G.; Verutes, G.; Wood, S.A.; Guerry, A.; Ruckelshaus, M.; Kareiva, P.; Lacayo, M.; Silver, J.M. Coastal habitats shield people and property from sea-level rise and storms. *Nat. Clim. Chang.* **2013**, *3*, 913–918. [CrossRef]
7. Yu, K.; Hu, C.; Muller-Karger, F.E.; Lu, D.; Soto, I. Shoreline changes in west-central Florida between 1987 and 2008 from Landsat observations. *Int. J. Remote Sens.* **2011**, *32*, 8299–8313. [CrossRef]
8. Li, W.; Gong, P. Continuous monitoring of coastline dynamics in western Florida with a 30-year time series of Landsat imagery. *Remote Sens. Environ.* **2016**, *179*, 196–209. [CrossRef]
9. Tamassoki, E.; Amiri, H.; Soleymani, Z. Monitoring of shoreline changes using remote sensing (case study: Coastal city of Bandar Abbas). In Proceedings of the IOP Conference Series: Earth & Environmental Science, Kuala Lumpur, Malaysia, 22–23 April 2014; p. 12023.
10. Dewi, R.S.; Bijker, W.; Stein, A.; Marfai, M.A. Fuzzy classification for shoreline change monitoring in a part of the northern coastal area of java, Indonesia. *Remote Sens.* **2016**, *8*, 190. [CrossRef]
11. Ghosh, M.K.; Kumar, L.; Roy, C. Monitoring the coastline change of Hatiya Island in Bangladesh using remote sensing techniques. *ISPRS J. Photogramm. Remote Sens.* **2015**, *101*, 137–144. [CrossRef]
12. Chen, L.C. Detection of shoreline changes for tideland areas using multi-temporal satellite images. *Int. J. Remote Sens.* **1998**, *19*, 3383–3397. [CrossRef]
13. Di, K.; Wang, J.; Ma, R.; Li, R. Automatic shoreline extraction from high-resolution IKONOS satellite imagery. In Proceedings of the ASPRS 2003 Annual Conference, Anchorage, AK, USA, 5–9 May 2003. Available online: https://www.researchgate.net/profile/Kaichang_Di/publication/241058589_Automatic_shoreline_extraction_from_high_resolution_IKONOS_satellite_imagery/links/004635383f740ac468000000.pdf (accessed on 1 March 2017).
14. Puissant, A.; Lefevre, S.E.B.; Weber, J. Coastline extraction in VHR imagery using mathematical morphology with spatial and spectral knowledge. In Proceedings of the SPRS Congress Beijing 2008, Beijing, China, 3–11 July 2008; pp. 1305–1310.
15. Lee, J.; Jurkevich, I. Coastline detection and tracing in SAR images. *IEEE Trans. Geosci. Remote Sens.* **1990**, *28*, 662–668.
16. Niedermeier, A.; Romaneessen, E.; Lehner, S. Detection of coastlines in SAR images using wavelet methods. *IEEE Trans. Geosci. Remote Sens.* **2000**, *38*, 2270–2281. [CrossRef]
17. Liu, H.; Jezek, K.C. A complete high-resolution coastline of Antarctica extracted from orthorectified Radarsat SAR imagery. *Photogramm. Eng. Remote Sens.* **2004**, *70*, 605–616. [CrossRef]
18. Liu, H.; Wang, L.; Sherman, D.J.; Wu, Q.; Su, H. Algorithmic foundation and software tools for extracting shoreline features from remote sensing imagery and LiDAR data. *J. Geogr. Inf. Syst.* **2011**, *3*, 99–119. [CrossRef]
19. Dellepiane, S.; de Laurentiis, R.; Giordano, F. Coastline extraction from SAR images and a method for the evaluation of the coastline precision. *Pattern Recogn. Lett.* **2004**, *25*, 1461–1470. [CrossRef]
20. Baselice, F.; Ferraioli, G. Unsupervised coastal line extraction from SAR images. *IEEE Geosci. Remote Sens.* **2013**, *10*, 1350–1354. [CrossRef]
21. Du, Z.; Li, W.; Zhou, D.; Tian, L.; Ling, F.; Wang, H.; Gui, Y.; Sun, B. Analysis of Landsat-8 OLI imagery for land surface water mapping. *Remote Sens. Lett.* **2014**, *5*, 672–681. [CrossRef]
22. Ryu, J.; Won, J.; Min, K.D. Waterline extraction from Landsat TM data in a tidal flat: A case study in Gomso Bay, Korea. *Remote Sens. Environ.* **2002**, *83*, 442–456. [CrossRef]
23. Chen, S.; Chen, L.; Liu, Q.; Li, X.; Tan, Q. Remote sensing and GIS-based integrated analysis of coastal changes and their environmental impacts in Lingding Bay, Pearl River Estuary, South China. *Ocean Coast. Manag.* **2005**, *48*, 65–83. [CrossRef]
24. El-Asmar, H.M.; Hereher, M.E. Change detection of the coastal zone east of the Nile Delta using remote sensing. *Environ. Earth Sci.* **2011**, *62*, 769–777. [CrossRef]
25. Cui, B.; Li, X. Coastline change of the Yellow River estuary and its response to the sediment and runoff (1976–2005). *Geomorphology* **2011**, *127*, 32–40. [CrossRef]
26. Mcfeeters, S.K. The use of the Normalized Difference Water Index (NDWI) in the delineation of open water features. *Int. J. Remote Sens.* **1996**, *17*, 1425–1432. [CrossRef]
27. Jain, S.K.; Singh, R.D.; Jain, M.K.; Lohani, A.K. Delineation of flood-prone areas using remote sensing techniques. *Water Resour. Manag.* **2005**, *19*, 333–347. [CrossRef]

28. Hui, F.; Xu, B.; Huang, H.; Yu, Q.; Gong, P. Modelling spatial-temporal change of Poyang Lake using multitemporal Landsat imagery. *Int. J. Remote Sens.* **2008**, *29*, 5767–5784. [CrossRef]
29. Xu, H. Modification of normalised difference water index (NDWI) to enhance open water features in remotely sensed imagery. *Int. J. Remote Sens.* **2006**, *27*, 3025–3033. [CrossRef]
30. Wang, Y.; Huang, F.; Wei, Y. Water body extraction from Landsat ETM+ image using MNDWI and KT transformation. In Proceedings of the IEEE 2013 21st International Conference on Geoinformatics, Kaifeng, China, 20–22 June 2013; pp. 1–5.
31. Shen, L.; Li, C. Water body extraction from Landsat ETM+ imagery using adaboost algorithm. In Proceedings of the IEEE 2010 18th International Conference on Geoinformatics, Beijing, China, 18–20 June 2010; pp. 1–4.
32. Li, L.; Li, Y.; Liu, K.; Wang, P. The assessment and influence factors analysis of development level of node cities on the maritime silk route. In Proceedings of the 2016 International Conference on Education, Management Science and Economics, Beijing, China, 28–29 May 2016; Atlantis Press: Amsterdam, The Netherlands, 2016; pp. 478–484.
33. Yang, H. Definition of the management boundary between river and sea in Ningbo. *J. Mar. Sci.* **2009**, *27*, 64–75. (In Chinese)
34. Ni, H.; Yi, B.; Yin, J.; Fang, T.; He, T.; Du, Y.; Wang, J.; Zhang, H.; Xie, L.; Ding, Y.; et al. Epidemiological and etiological characteristics of hand, foot, and mouth disease in Ningbo, China, 2008–2011. *J. Clin. Virol.* **2012**, *54*, 342–348. [CrossRef] [PubMed]
35. Chen, J.; Liu, C.; Zhang, C.; Walker, H.J. Geomorphological development and sedimentation in qiantang estuary and Hangzhou bay. *J. Coast. Res.* **1990**, *3*, 559–572.
36. Yang, H.; Xue, B.; Jin, L.; Zhou, S.; Liu, W. Polychlorinated biphenyls in surface sediments of Yueqing Bay, Xiangshan Bay, and Sanmen Bay in East China Sea. *Chemosphere* **2011**, *83*, 137–143. [CrossRef] [PubMed]
37. Huang, S.C.; Lou, H.F.; Xie, Y.L.; Hu, J.J. Hydrodynamic environment and its effects in the Xiangshan Bay. In Proceedings of the International Conference on Estuaries and Coasts, Hangzhou, China, 9–11 Novermber 2003; pp. 9–11.
38. Li, W.; Yang, H.; Gao, Q.; Pan, H.; Yang, H. Residues of organochlorine pesticides in water and suspended particulate matter from Xiangshan Bay, East China Sea. *Bull. Environ. Contam. Toxicol.* **2012**, *89*, 811–815. [CrossRef] [PubMed]
39. Li, W.; Yu, T.; Li, J.; Chen, P.; Chen, Y. Suitability evaluation of land use in coastal zones: A case study in southern Hangzhou Bay. *Geogr. Res.* **2015**, *34*, 701–710. (In Chinese)
40. Chen, X.; Zhang, J.; Ma, Y.; Cui, T. Monitoring and analysis of coastline changes of the Sanmen Bay with remote sensing during the past 40 years. *Mar. Sci.* **2015**, *39*, 43–49. (In Chinese)
41. Boak, E.H.; Turner, I.L. Shoreline definition and detection: A review. *J. Coast. Res.* **2005**, *214*, 688–703. [CrossRef]
42. Pardo-Pascual, J.E.; Almonacid-Caballer, J.; Ruiz, L.A.; Palomar-Vázquez, J. Automatic extraction of shorelines from Landsat TM and ETM+ multi-temporal images with subpixel precision. *Remote Sens. Environ.* **2012**, *123*, 1–11. [CrossRef]
43. Yang, C.; Cai, X.; Wang, X.; Yan, R.; Zhang, T.; Zhang, Q.; Lu, X. Remotely Sensed Trajectory Analysis of Channel Migration in Lower Jingjiang Reach during the Period of 1983–2013. *Remote Sens.* **2015**, *7*, 16241–16256. [CrossRef]
44. Du, Y.; Zhang, Y.; Ling, F.; Wang, Q.; Li, W.; Li, X. Water bodies' mapping from sentinel-2 imagery with modified normalized difference water index at 10-m spatial resolution produced by sharpening the SWIR band. *Remote Sens.* **2016**, *8*, 354. [CrossRef]
45. Li, W.; Du, Z.; Ling, F.; Zhou, D.; Wang, H.; Gui, Y.; Sun, B.; Zhang, X. A comparison of land surface water mapping using the normalized difference water index from TM, ETM+ and ALI. *Remote Sens.* **2013**, *5*, 5530–5549. [CrossRef]
46. Xu, H. A study on information extraction of water body with the modified normalized difference water index (MNDWI). *J. Remote Sens.* **2005**, *5*, 589–595. (In Chinese)
47. Ji, L.; Zhang, L.; Wylie, B. Analysis of dynamic thresholds for the normalized difference water index. *Photogramm. Eng. Remote Sens.* **2009**, *75*, 1307–1317. [CrossRef]
48. Otsu, N. A threshold selection method from gray-level histograms. *Automatica* **1975**, *11*, 23–27. [CrossRef]
49. Sarkar, N.; Chaudhuri, B.B. An efficient differential box-counting approach to compute fractal dimension of image. *IEEE Trans. Syst. Man Cybern.* **1994**, *24*, 115–120. [CrossRef]

50. Zhu, X.; Cai, Y.; Yang, X. On fractal dimensions of China's coastlines. *Math. Geol.* **2004**, *36*, 447–461.
51. Smith, M.J.; Cromley, R.G. Measuring historical coastal change using GIS and the change polygon approach. *Trans. GIS* **2012**, *16*, 3–15. [CrossRef]
52. Thieler, E.R.; Himmelstoss, E.A.; Zichichi, J.L.; Ergul, A. *Digital Shoreline Analysis System (DSAS) Version 4.0-An. ArcGIS Extension for Calculating Shoreline Change*; Open-File Report 2008–1278 (Updated for Version 4.3); U.S. Geological Survey: Woods Hole, MA, USA, 2009; pp. 1–81.
53. Louati, M.; Saïdi, H.; Zargouni, F. Shoreline change assessment using remote sensing and GIS techniques: A case study of the Medjerda delta coast, Tunisia. *Arab. J. Geosci.* **2015**, *8*, 4239–4255. [CrossRef]
54. Zhang, Y.; Li, X.; Zhang, J.; Song, D. A study on coastline extraction and its trend based on remote sensing image data mining. *Abstr. Appl. Anal.* **2013**, *2013*, 1–6. [CrossRef]
55. Wang, T.; Zhang, G.; Li, D.; Tang, X.; Jiang, Y.; Pan, H.; Zhu, X.; Fang, C. Geometric accuracy validation for ZY-3 satellite imagery. *IEEE Geosci. Remote Sens.* **2014**, *11*, 1168–1171. [CrossRef]
56. Kaergaard, K.; Fredsoe, J. A numerical shoreline model for shorelines with large curvature. *Coast. Eng.* **2013**, *74*, 19–32. [CrossRef]
57. Young, I.T. Proof without prejudice: Use of the Kolmogorov-Smirnov test for the analysis of histograms from flow systems and other sources. *J. Histochem. Cytochem.* **1977**, *7*, 935–941. [CrossRef] [PubMed]
58. Xie, D.; Wang, Z.; Gao, S.; de Vriend, H.J. Modeling the tidal channel morphodynamics in a macro-tidal embayment, Hangzhou Bay, China. *Cont. Shelf Res.* **2009**, *29*, 1757–1767. [CrossRef]